Toward High Capacity Molecular Communications Using Sequential Vortex Rings

Mahmoud Abbaszadeh, Peter J. Thomas, and Weisi Guo

***Abstract*—Molecular signal coherence in fluid dynamic channels is severely hindered by mass, momentum, and turbulent diffusive forces. The combination of such forces causes long molecular tails, which results in severe inter-symbol-interference (ISI) and limits the achievable symbol rate. Here, we propose to modulate information symbols into stable vortex ring structures to minimize ISI. Each vortex ring can propagate approximately 100× the diameter of the transmission nozzle without losing its compact shape. First, we show that the ISI from sequential transmissions is minimal and reduces rapidly with distance after transmission. This is the opposite effect to conventional molecular puffs undergoing advection-diffusion, whereby ISI increases with distance. Second, we show that by maintaining a coherent signal structure, the signal-to-inference ratio is 211× higher over conventional puffs. Also, we demonstrate the vortex ring using a proof-of-concept prototype. The results point toward a promising pathway for higher capacity channels.**

***Index Terms*—Molecular communication, channel capacity, vortex ring, turbulent diffusion.**

I. Introduction

CONVENTIONAL molecular signals are represented by discontinuous molecular puffs that are ejected into a fluid or gas channel. After ejection, at the macro-scale, the signal is subject to various pressure, velocity, sheer stress gradients, as well as reaction forces. The coupling relationships between these forces and the flow rate are well described by the Navier-Stokes (NS) equations [1]. Existing literature in molecular communications has predominantly used isotropic diffusion-advection channel models due to their tractable expressions [2], assuming a Péclet number below 1 (e.g., mass diffusion dominates). Whilst this is reasonable for cell membranes and capillary blood flow, advection and external forces will dominate at larger-scales. Sheer stress between laminar flow layers leads to viscous momentum diffusion and turbulence will cause turbulent diffusion [3].

A. Vortex Rings in Turbulence

Turbulence is not only inherently very difficult to model, but it also does not directly help us understand the communication capacity of the channel. Yet, we can take advantage of a certain structure called a *vortex ring*, that propagates well in turbulent fluid channels. The vortex ring retains spatial structure through its rotational momentum and has a sharper concentration time profile than a standard puff - see Fig. 1. This has the potential to significantly reduce inter-symbol-interference (ISI) from sequential transmissions and as such allow us to transmit at a higher symbol rate. The vortex ring core is a torus shaped fluid or gas structure, that retains shape (e.g., mitigates dispersion) for long propagation distances (typically 100× *nozzle diameter*) [4] - see Fig. 2. Each vortex ring is a region, where the molecules mostly spin around an axis in a closed loop. Finally, it should be noted that one of the possible application of the vortex rings is the Line-of-sight (LOS) communication.

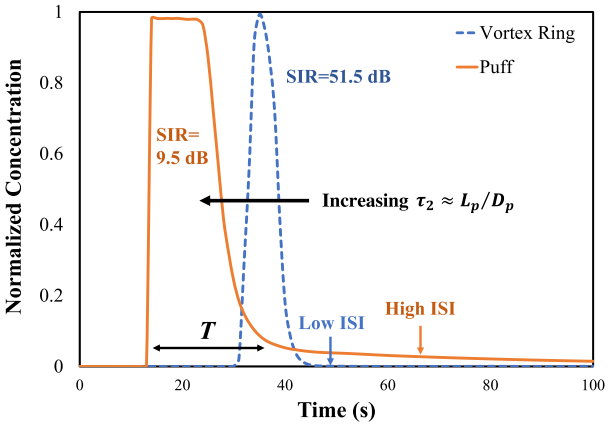

Fig. 1. Concentration (normalised) time profile at receiver for a standard puff (large ISI) and a vortex ring (small ISI).

B. Contribution

In this letters, we will use both simulation and experimentation to outline how vortex rings are generated and how they effectively mitigate ISI over long distances. In Section II, we present the theoretical structure of a vortex ring and the transmitter design required to generate it. In Section IV, we show the propagation life cycle of sequential vortex rings in comparison to conventional molecule puffs and demonstrate it using an experimental proof-of-concept test-bed. We analyze the SIR profile for different configuration parameters and discuss capacity scalability potential. Finally, we observe the effects of each vortex ring on the others in a series of sequential vortex rings and the way they can go through the channel with minimum interference.

II. Vortex Ring Structure & Generation

A vortex ring is a bounded region of vorticity in which the vortex lines form closed loops [5]. Vortex rings which

Manuscript received May 24, 2018; revised September 2, 2018 and November 27, 2018; accepted December 10, 2018. Date of publication December 17, 2018; date of current version April 19, 2019. This work was supported by U.S. AFOSR under Grant FA9550-17-1-0056. The associate editor coordinating the review of this paper and approving it for publication was C. T. T. Chou. *(Corresponding author: Weisi Guo.)*

The authors are with the School of Engineering, University of Warwick, Coventry CV4 7AL, U.K. (e-mail: weisi.guo@warwick.ac.uk).

Digital Object Identifier 10.1109/TMBMC.2018.2887238

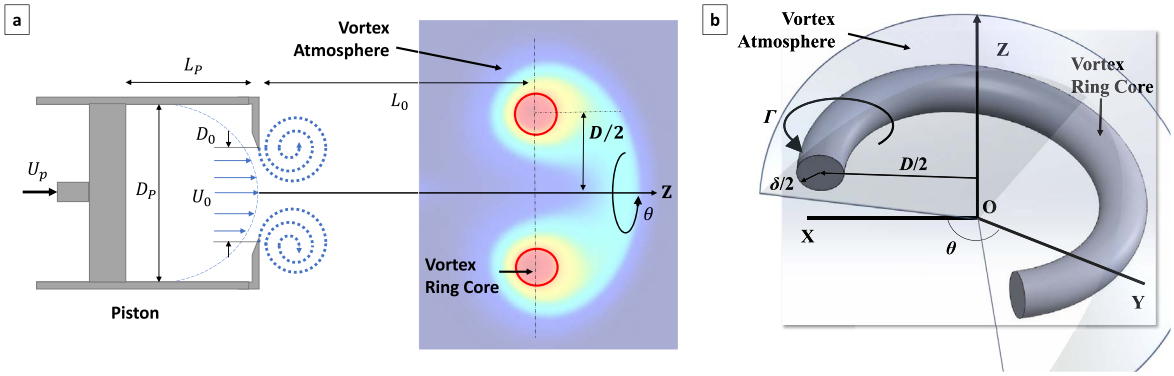

Fig. 2. (a) Illustration of transmitter piston design to generate vortex ring. (b) Illustration of vortex ring core properties and its orientation in cylindrical coordinates with a surrounding vortex atmosphere.

are circular, stable and have the ability to retain molecular information in a self-sustained structure. It is worth noting that the vortex core can become wavy (Widnall instability) at some point during its existence depending on conditions. The general properties of every vortex ring can be observed in Fig. 2, where the vortex ring core has diameter of D (approximately $1.3\times$ the nozzle diameter D_0) and the bulk of vorticity in the region has diameter of δ. There is also a small atmosphere surrounding the core - see Fig. 2b.

In order to design the transmitter that can generate a vortex ring, careful consideration is needed - see Fig. 2a. First, the molecules inside the piston must be subject to a sufficient sheer stress profile such that vortices are generated. This occurs when the molecules are pushed out at a sufficiently high Reynolds number, generating a vortex ring head. In the case of vortex rings, the Reynolds number is given by $\mathrm{Re}_\Gamma = \frac{\Gamma}{\nu}$ where ν is the kinematic viscosity of the ejected fluid and Γ is the circulation given in Eq. (1). To find Re_Γ, we first need to define the inertial forces inside a region of vorticity, with molecules spinning around an imaginary axis in a closed loop.

$$\Gamma = \int_S \nabla \times \mathbf{u}\, \mathrm{d}\mathbf{S} = \oint_l \mathbf{u}\, \mathrm{d}\mathbf{l}, \tag{1}$$

where $\mathbf{S}$ is a closed surface which is bounded by line $\mathbf{l}$ and $\mathbf{u}$ is the velocity field in the flow domain.

To generate the vortex ring, a prescribed axial velocity can be defined at the transmitter to simulate the motion of the piston and also to define the vorticities at the edge of the piston [6]:

$$V_z(t, r) = V_0(t)\, V_{zb}(r), \tag{2}$$

where $V_0(t)$ is the time-variant velocity program that expresses the piston motion and given by [6]:

$$V_0(t) = \begin{cases} \frac{U_p}{2}\left\{1 + \tanh\left[\frac{5}{\tau_1}(t - \tau_1)\right]\right\}, & t < \tau_1 + \frac{\tau_2}{2} \\ \frac{U_p}{2}\left\{1 + \tanh\left[\frac{5}{\tau_1}(\tau_1 + \tau_2 - t)\right]\right\}, & t \geq \tau_1 + \frac{\tau_2}{2} \end{cases} \tag{3}$$

where U_p is the maximum piston velocity. The parameter τ_1 is a short-time acceleration/deceleration of the impulsive piston, and the value of the τ_2 is equal to the stroke ratio ($\tau_2 \approx L_p/D_P$). In the stroke-ratio formula, L_p is the stroke length, and if the piston reaches the end of the cylinder, we have maximum stroke ratio as shown in Fig. 2a.

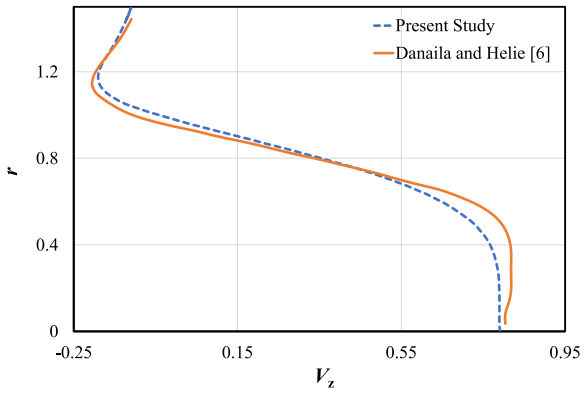

Fig. 3. Validation of present study with Danaila and Helie's study [6].

Also, V_{zb} is the classical hyperbolic tangent profile which has been derived from the experiment and represents the thickness of the vorticity layer at the edge of the cylinder [7]:

$$V_{zb}(r) = \frac{1}{2}\left\{1 + \tanh\left[\frac{1}{2\delta_w}\left(\frac{D_p}{2r} - \frac{2r}{D_p}\right)\right]\right\}, \tag{4}$$

where δ_w is the dimensionless thickness of vorticity layer at the transmitter and it is considered 0.05 in this letter which shows a thin vorticity layer. The diameter of the piston is D_p and r is the radial distance from the center of the inlet.

The only theoretical insight comes from the piston stroke ratio. For $\boldsymbol{L_p/D_p \geq 4}$, the leading vortex ring is followed by an active trailing jet-like region [8], and as the stroke ratio increases, more ejected fluid stays behind the leading vortex ring. Actually, the maximum circulation that a vortex ring can attain, occurs at $L_p/D_p \approx 4$ (which is refered to as "formation number") [8] and after that, as the stroke ratio increases, the leading vortex ring sheds excessive ejected fluid behind. Also, all the quantities in this letter are normalized by D_p and U_p as the characteristic length and velocity, respectively. Also, D_p/U_p is used to normalize the time.

Moreover, in order to ensure the accuracy of our numerical program, we simulate the Danaila and Helie's [6] injector and present the results in Fig. 3 where a good agreement can be observed between our results and Danaila and Helie's [6] study. In this figure, r is the normalized radial distance from the center of piston outlet and V_z is the normalized axial velocity.

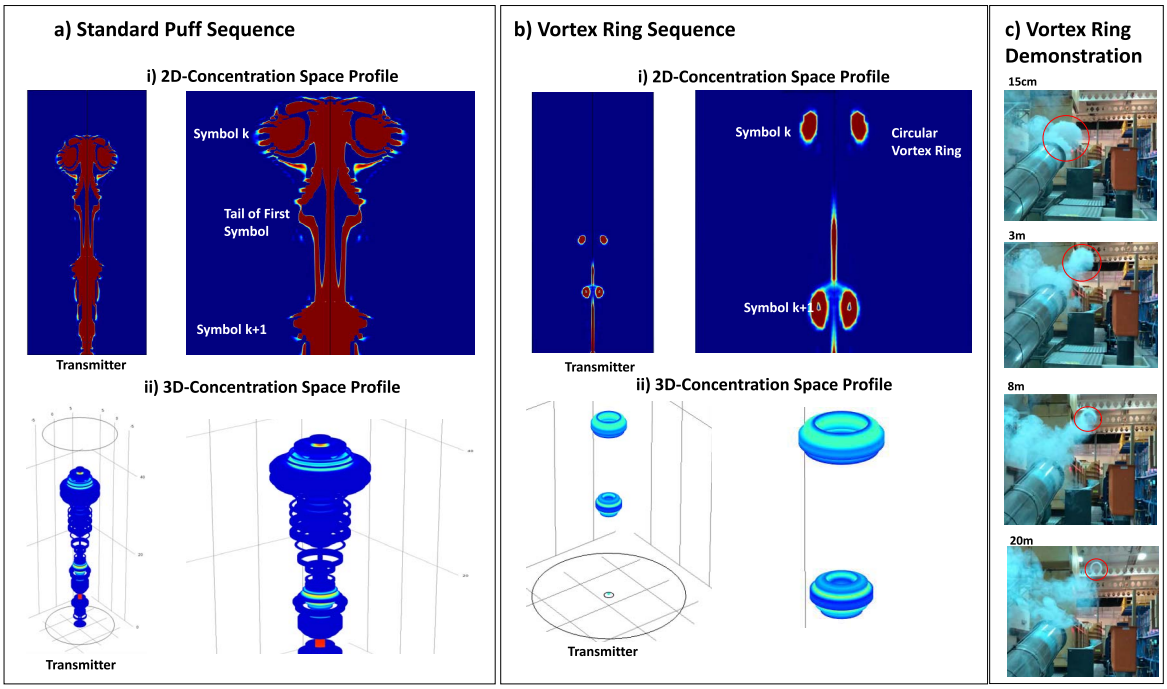

Fig. 4. Sequential symbols transmitted: (a) puffs, (b) vortex rings, and (c) experimentation of vortex rings.

TABLE I
SIMULATION PARAMETERS

Variable	Value
Stroke Ratio, L_p/D_p	2 - vortex ring, 14 - Puff
Maximum Injection Velocity, U_P	2.5 m/s at $t = 0$
Dynamic Viscosity of water, ν	8.9×10^{-4} Pa.s
Transmit Concentration, c_0	2.5 mol/m^3
Pulse Width, T_0	2.29 s
Symbol Period, T	16 s
Simulation Space	$50D_p$ long, $20D_p$ wide

III. RESULTS & DISCUSSION

A. Method and Parameters

In order to fully model turbulent diffusion with an anisotropic and time-varying velocity profile, the **Reynolds-averaged Navier-Stokes (RANS)** equations needs to be considered [3]:

$$c\overline{u}_j \frac{\partial \overline{u}_i}{\partial x_j} = c\overline{f}_i + \frac{\partial}{\partial x_j}\left[-\overline{p}\delta_{ij} + \mu\left(\frac{\partial \overline{u}_i}{\partial x_j} + \frac{\partial \overline{u}_j}{\partial x_i}\right) - c\overline{u_i' u_j'}\right]. \quad (5)$$

where c represents density or concentration which depends on pressure, velocity, and sheer stress gradients. The over-bar represents time-averaged values, and μ is dynamic viscosity of the fluid. The term $c\overline{u}_j \frac{\partial \overline{u}_i}{\partial x_j}$ represents the change in mean momentum of the fluid element owing to the unsteadiness in the mean flow and the convection by the mean flow. This is balanced by the mean body force $\overline{f}_i$, the isotropic stress from the pressure field $\overline{p}\delta_{ij}$, the viscous stresses, and apparent stress $-c\overline{u_i' u_j'}$ owing to the fluctuating velocity field (Reynolds stress). Whilst there are statistical approximate solutions in the form of eddy diffusivity, general tractability is still a challenge for modeling turbulent diffusion processes. This is the reason why finite-element simulation and experimentation is used.

B. Transmission

1) Simulation: The simulations are conducted using industrial standard COMSOL software with the Computational Fluid Dynamics (CFD) and Chemical Species Transport modules coupled. The simulation parameters are given in Table I. We shoot a sequence of conventional puffs and vortex rings and show their forward concentration (space domain) profiles in Fig. 4. Each received signal is given by: $c(t) = \sum_k^K a_k h(t - kT)$, where a is 1 or 0 (OOK), T is the symbol period, and the channel $h(.)$ is a complex fluid dynamic channel described by the aforementioned RANS equations to solve for the turbulence effects. In reality and for detection purposes, we can employ **particle image velocimetry (PIV) and planar laser induced florescence (PLIF)** techniques which is a passive receiver and by using laser, camera, and florescence dye we can observe the concentration of molecules [9]. The second way of detection is using an **array of chemical sensors** which is an active way of detection. Both of the aforementioned ways, recover the spatio-temporal profiles.

It is worth noting that under RANS, these are the averaged profiles over a small simulation element. We assume that the vortex rings are sufficiently separated such that each behaves independently, but will explore mutual interactions in the future, especially the effects of leap-frogging and the leading vortex ring's drag.

Puff Sequence - Fig. 4a-i shows the concentration profile, where there is a rapid deterioration in concentration structure and intensity over distance. As such, the tail from prior symbols leads to strong ISI. Fig. 4a-ii is the 3D concentration profile and reveals that there is not a specific circular ring in the environment and the tail of the puff remains in the environment for a whole period of transmission.

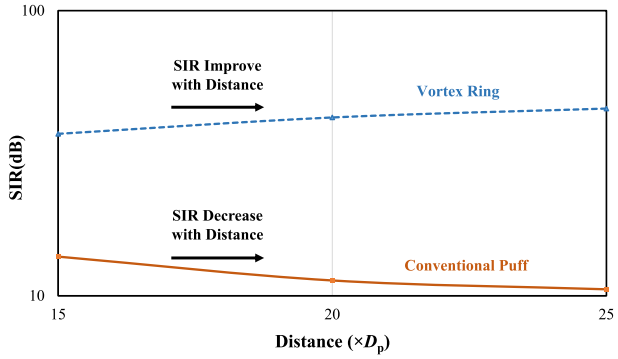

Fig. 5. SIR as a function of transmission distance for a standard puff (SIR decays with distance) and a vortex ring (SIR increases with distance).

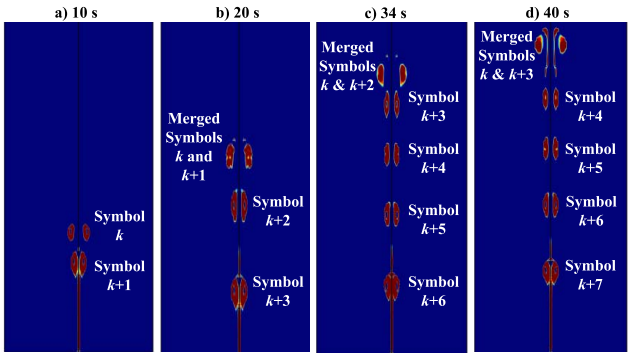

Fig. 6. Demonstration of sequential vortex ring symbol transmission observed at different times.

Vortex Ring Sequence - The results in Fig. 4b-i show that the vortex ring core has a high concentration compared to the quiescent environment and maintains this into distance. This means that the vortex ring is carrying the momentum of the transmitter and is dominant in the way it propagates through the environment. Fig. 4b-ii shows the concentration profile in three dimensions, where high concentration is maintained and the ISI effects are small. Overall, we observe that the ISI tail is significantly lower for the vortex ring (as shown in the concentration time profile in Fig. 1).

2) Experimentation: We also present a proof-of-concept demonstration of the vortex ring, being shot 20m into an uncontrolled environment in Fig. 4c. We have a 0.2 m diameter vortex canon that is shooting a vortex ring captured on a slow motion camera. The red rings label the location of the vortex ring as it propagates away from the canon. The vortex ring becomes clearer as it moves into the distance.

C. Signal-to-Interference (SIR) Ratio

For the received signal with empirical response $h(t)$, we define the signal $S = \int_0^T h(t)\mathrm{d}t$ as the aggregate peak concentration values detected over symbol period T. We define the ISI as $I = \sum_k \int_0^T h(t+kT)\mathrm{d}t = \int_T^{+\infty} h(t)\mathrm{d}t$ as the remaining tail concentration $t > T$. For a single symbol, the resulting SIR is as follows - see Fig. 1: (1) Vortex Ring: +51.5dB, and (2) Puff: +9.5dB. We can see approximately a 211× improvement when the vortex ring is compared to the puff. As shown in Fig. 5, we can see that SIR as a function of transmission distance for a standard puff (SIR decays with distance) and a vortex ring (SIR increases with distance).

D. Sequential Vortex Rings

In this section, we transmitted eight vortex rings in order to observe the effects of each vortex ring on the others and to see how a sequence of information can be carried by vortex rings with minimum interference and maximum symbol rate. Parameters: $U_p = 5$ m/s and the $L_p/D_p = 1$. The vortex rings concentration profiles are displayed in Fig. 6 at four different time snapshots after transmission. After 10s (Fig. 6-a), we can see that the second vortex ring $k+1$ catches up with the first k, and merge at 20s. This also repeats for symbols $k+2$ and $k+3$. As a consequence, when the symbol period is small, the first four vortex rings will merge together (Fig. 6-c/d). However, subsequent vortex rings remain separated and can be detected coherently. This seems to indicate that an initial sacrifice of 4 symbols is needed to clear the channel up to the $50D_p$ critical distance [4], allowing subsequent symbols to propagate coherently. Any longer distances and the vortex rings become unstable. As such, we may regard the first 4 symbols as pilot symbols to sense the channel or communicate non-data bearing information. In contrast, if we consider the receiver at a critical distance (for example in this simulation setup, the critical distance is $10D_p$), the merging would not be happened and the receiver can detect each symbol separately.

IV. Conclusion & Future Work

In this letter, we demonstrated how packing information in vortex rings can effectively mitigate ISI using computation fluid dynamic numerical simulation and proof-of-concept experimentation. Not only do we show that ISI has been reduced by one order of magnitude compared to standard puff emissions, but we also show that ISI actually reduces with distance in the far field. In future work, we will explore the potential for longer distance guided transmission and capacity scaling using parallel vortex rings in MIMO.

References

[1] B. D. Unluturk and I. F. Akyildiz, "An end-to-end model of plant pheromone channel for long range molecular communication," *IEEE Trans. Nanobiosci.*, vol. 16, no. 1, pp. 11–20, Jan. 2017.

[2] W. Guo *et al.*, "Molecular communications: Channel model and physical layer techniques," *IEEE Wireless Commun.*, vol. 23, no. 4, pp. 120–127, Aug. 2016.

[3] P. J. W. Roberts and D. R. Webster, "Turbulent diffusion," in *Environmental Fluid Mechanics-Theories and Application*. Reston, VA, USA: Amer. Soc. Civil Eng., 2002.

[4] M. A. Brend and P. J. Thomas, "Decay of vortex rings in a rotating fluid," *Phys. Fluids*, vol. 21, no. 4, 2009, Art. no. 044105.

[5] T. T. Lim and T. B. Nickels, "Vortex rings," in *Fluid Vortices*. Berlin, Germany: Springer, 1995, pp. 95–153.

[6] I. Danaila and J. Hélie, "Numerical simulation of the postformation evolution of a laminar vortex ring," *Phys. Fluids*, vol. 20, no. 7, 2008, Art. no. 073602.

[7] I. Danaila, C. Vadean, and S. Danaila, "Specified discharge velocity models for numerical simulations of laminar vortex rings," *Theor. Comput. Fluid Dyn.*, vol. 23, no. 5, p. 317, 2009.

[8] M. Gharib, E. Rambod, and K. Shariff, "A universal time scale for vortex ring formation," *J. Fluid Mech.*, vol. 360, pp. 121–140, Apr. 1998.

[9] H. Hu, T. Saga, T. Kobayashi, and N. Taniguchi, "Simultaneous velocity and concentration measurements of a turbulent jet mixing flow," *Ann. New York Acad. Sci.*, vol. 972, no. 1, pp. 254–259, 2002.